Coastal Dynamics 2017
Paper No. 190

LOCALLY VARYING INUNDATION CHARACTERISTICS ALONG COAST LINES OF BATANES INDUCED BY SUPER TYPHOON MERANTI

John Phillip Lapidez[1], Yoshimitsu Tajima[1], Jeane Camelo[2], Mizuka Saito[1], Yoshinao Matsuba[1], Takenori Shimozono[1], Marjorie Turiano[2], Dominic Bautista[2], and Eric Cruz[2]

Abstract

Super Typhoon Meranti, the strongest typhoon of 2016, caused serious damages in the Philippines. This paper discusses the characteristics of observed inundation and runup along the coast of Batanes in the north of the Philippines. WaveWatch III was applied for hindcast of wind-induced offshore waves and time-dependent linear mild-slope equations were applied for computations of nearshore waves accounting for topographic shading effects of Batan Island. Results show that the inundation pattern is reasonably explained by wind-induced offshore waves, shading effects of the island, and wave dissipation on the fringing reefs except the extraordinarily high inundation observed at the municipality of Ivana located in the southwestern tip of Batan. This site is also fronted by a convex-shaped reef with a narrow gap for navigation channel, which may have caused the observed local amplification of waves.

Key words: Meranti, Storm wave, Fringing reef, Infragravity wave

1. Introduction

Super typhoon Meranti, locally named Ferdie in the Philippines, is one of the strongest typhoons in record. The minimum pressure of Meranti was 890 hPa and its maximum 10-minute sustained winds was 220 km/h. For comparison, typhoon Tip (1979) which is regarded as the strongest typhoon recorded, had a minimum pressure of 870 hPa and maximum 10-minute sustained wind velocity of 260 km/h (Dunnavan & Diercks, 1980).

A post-disaster survey was conducted in the islands of Batanes, which is one of the most heavily impacted regions by Meranti. This study aims to investigate the variation of inundation levels along the coastlines of Batanes under the influence of the extreme typhoon event and to examine the effects of the fringing reefs and other various geographic features such as shoreline angles, and shading effects of the topography of the island on the observed runup and inundation levels.

1.1 Meteorological History of Super Typhoon Meranti

At 18:00 UTC on 8 September 2016, the Japan Meteorological Agency (JMA)[3] first identified Meranti as a Tropical Depression. And by 06:00 UTC of 10 September, the JMA upgraded the classification of Meranti to Tropical Storm which is defined to have the 10-minute sustained wind velocity within the range of 62–88 km/h. By the next day, Meranti started to move in the west-northwest direction and was posed to hit the north part of the Philippines. At 06:00 UTC of that day, Meranti was upgraded to Typhoon status by the JMA (10-min sustained winds: 118–156 km/h). At this point, Meranti underwent rapid intensification due to favorable environment conditions. At 06:00 UTC of 12 September, the Joint Typhoon Warning Center (JTWC)[4] upgraded Meranti to Super Typhoon status, with 1-minute maximum sustained winds has reached 285 km/h, placing it at Category 5 on the Saffir–Simpson scale while still rapidly intensifying. Finally, Meranti has

[1]Department of Civil Engineering, The University of Tokyo, Hongo 7-3-1, Bunkyo, Tokyo 113-8656, Japan. philliplapidez@coastal.t.u-tokyo.ac.jp
[2]Institute of Civil Engineering, University of the Philippines, Quezon City 1101 Philippines. eric.cruz@upd.edu.ph
[3]JMA is the official Regional Specialized Meteorological Center for the western Pacific Ocean.
[4]JTWC is a joint US Navy and US Air Force command responsible for the issuing of tropical cyclone warnings in the North West Pacific Ocean, South Pacific Ocean and Indian Ocean for U.S. government agencies.

reached its peak at around 12:00 UTC of 13 September while passing at the north of the Philippines. The JMA estimated Meranti's peak 10-minute sustained winds to be 220 km/h with a minimum central pressure of 890 hPa. JTWC also reported estimated peak 1-minute sustained winds of 305 km/h, firmly placing Meranti among the strongest typhoons in record (Joint Typhoon Warning Center, 2016).

Figure 1 shows the track of Super Typhoon Meranti with different colored circle markers indicating the wind speed values and Figure 2 shows the distribution of the wind speed and directions recorded at a reference point in Batan Island.

1.2 The Survey Location: Batanes Islands, Philippines

Between 15:00 and 18:00 UTC of September 13, Meranti, still being in the Super Typhoon category, passed north of the islands of Batanes as seen in Figure 1. Extreme waves and winds attacked Batanes, completely destroying 292 houses and partially collapsing another 932. Batanes is the northernmost province of the Philippines and is composed of several islands including Batan and Sabtang. The field survey was done in these two islands, with the majority of the data points in Batan Island. One important feature of this island is that it is surrounded by wide fringing reefs. Almost the entire length of the Batan coastline is fronted by

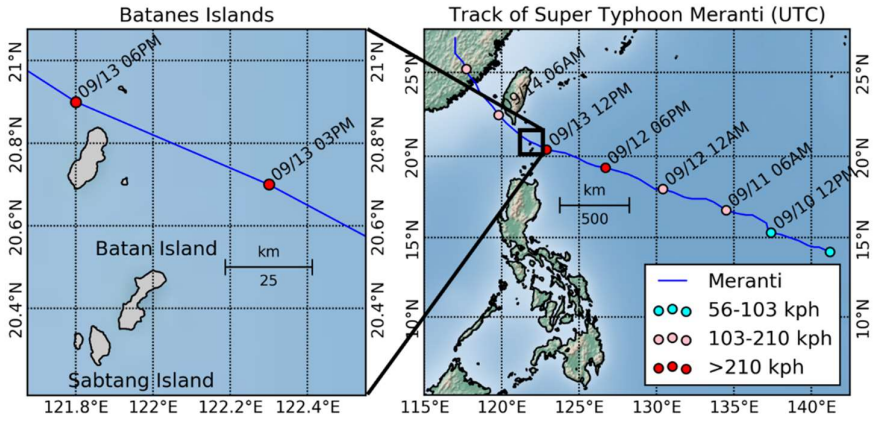

Figure 1. Track of Super Typhoon Meranti

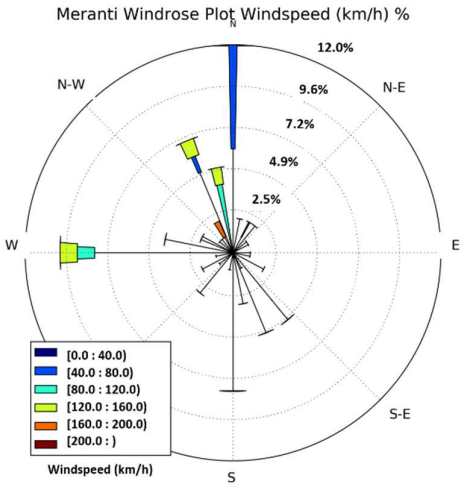

Figure 2. Wind rose plot showing the direction and wind speed of super typhoon Meranti [NOAA National Climatic Da ta Center, 2016]

fringing reefs. Figure 3 shows several satellite images of fringing reefs at different locations along the perimeter of Batan. The width of the reef varies largely at each site, ranging from less than 50 m up to more than 150 m. The average width of the reef at measured at all the survey locations is 95 m. One important task of the survey was to observe the height of runup and the peak water level of inundation on the beach fronted by fringing reef because previous studies have shown that fringing reefs have a significant influence on the transformation of the incoming waves both during normal and stormy wave conditions. In general, offshore reefs provide the beach protection by reducing the energy of the incoming waves. The waves are broken at the reef front and additional energy loss is incurred due to the higher bottom friction of the reefs (Hardy & Young, 1996), (Pe´quignet, et al., 2011). However, during extreme conditions such as during typhoons, the increased water level on the reef lowers its resonant period which can possibly result to resonant amplification of infragravity waves (Pe´quignet, et al., 2009). The effect of this phenomenon was observed at the coast of Eastern Samar during typhoon Haiyan (2013) resulting to extreme coastal flooding and significant damages to coastal villages (Tajima, et al., 2014 and 2016; and Shimozono, et al., 2015).

2. Survey Methodology

The post disaster survey was conducted at the islands of Batan and Sabtang from 9 to 12 of Oct 2016, about a month after the devastation of Meranti. The survey consisted of two primary methods in acquisition of wave runup and inundation data: interviews from local residents residing near the coast, and examination of inundation evidences left at the sites. Most residents of the coastal communities stayed at their houses during the typhoon, and therefore have a reliable recollection about the event. Residents were interviewed about the estimated height of rise of the mean sea level, extent and height of wave run-up, directions of approaching wind and waves, and the time of the occurrence of the event. In the coastal areas that were uninhabited, evidences of wave run-up were investigated through observation or examination of debris lines of driftwood, freshly eroded roots of coconut trees near the coastline, scour around structures, and damages on structures. Other relevant information such as important geologic features and existence of reefs in the locality were also noted. Actual survey photos are shown in Figure 4.
Figure 5 shows the schematic diagram of the measurements taken at each site. The vertical measurements a(R), a(I), and a(V) were all referred from the mean sea level at the time of the survey while b(I) and b(V) were directly measured from the ground level. The values were then adjusted to the water levels at the time of the event by considering the actual tide level at the estimated time of the event of inundation or runup. A

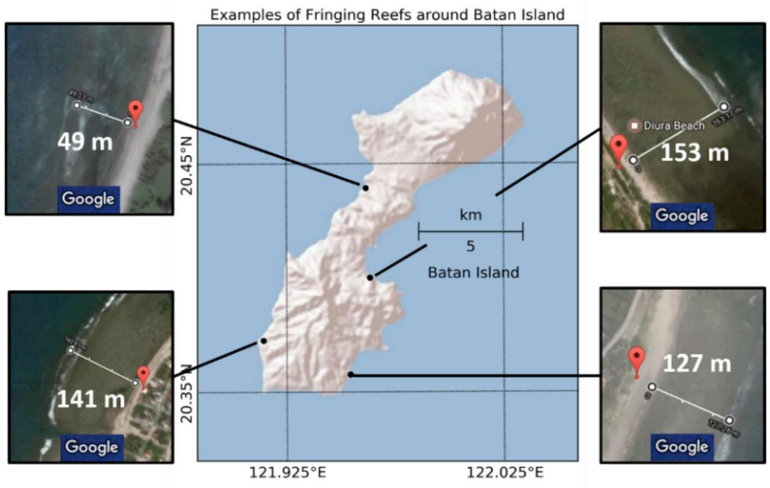

Figure 3. Some satellite images of fringing reefs fronting the inundation survey locations (Images taken from Google Maps)

more detailed account of the methodology of the post-disaster survey and complete information of measurements can be found in the report of Tajima et al. (2017).

3. Survey Results

Following the interview and identification of run-up evidence, measurements were taken at 37 sites in total along the coastlines of islands of Batan and Sabtang. A summary of all the collected data can be found at Tajima et al. (2017). Figure 6 shows the spatial distribution of the same set of data with the measured elevation of runup (blue bars), witnessed water levels in the inundated areas (red bars) and range of instantaneous fluctuations witnessed by local residents (black bars). Elevations presented are referred from the mean lower low water (MLLW). The collected data shows a general trend that the coastlines facing the north direction experienced higher wave run-up and inundation. The highest runup elevation, 6.3 m, was observed at site 37, while the highest inundation level, 6.1 m, was observed at site 16; both sites located at the north-facing coast of the island of Batan. This is consistent with the dominant wind direction of Meranti, as seen in the wind rose plot in **Error! Reference source not found.**ure 2. On the other hand, coastlines that were shielded by other land masses such as the beach in the south of Batan partly shielded by Sabtang Island experienced lower values of runup.

Figure 4. Pictures of: (a) debris lines; (b) exposed roots of coconut trees; (c) scour around a house; and (d) collapsed seawall

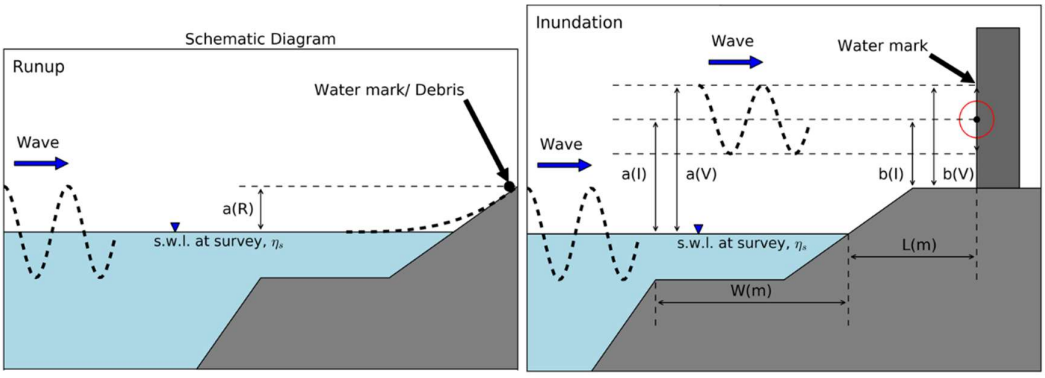

Figure 5. Schematic diagram of the survey measurements. (Left): a(R) is the runup height indicated by water mark or debris measured from local sea water level, η_s. (Right): a(I) and b(I) are inundation heights measured from sea level and ground level respectively. a(V) and b(V) are the maximum water level including fluctuating water surface. W is the width of the fringing reef and L is the distance from the shoreline to the target.

4. Wave Deformation Around Batan Island

First, a wave hindcast was performed using WaveWatch III. The typhoon wind model was constructed using the best track data of Meranti from JMA together with the wind and pressure distribution functions proposed by Mitsuta & Fujii (1987). The drag coefficient, C_d, used in the wave hindcast was adopted from Oey et al. (2006) which fits data for low-to-moderate winds with data for high wind speeds. The model was run on a 30 second gridded region covering the vicinity of the Batanes Islands. Snapshots of the spatial distribution of significant wave height, H_s, at different times computed by the WaveWatch III wave hindcast are shown in Figure 7.

Second, a numerical model based on the mild-slope equations was constructed to study the wave deformation characteristics around the island of Batan. The results of the wave hindcast were used as boundary condition to this model. This is necessary because WaveWatch III is not capable of accounting for wave diffraction, which is very important to consider especially at the nearshore. The subsequent simulation considered the two-dimensional wave deformation processes refraction and diffraction. The purpose of the

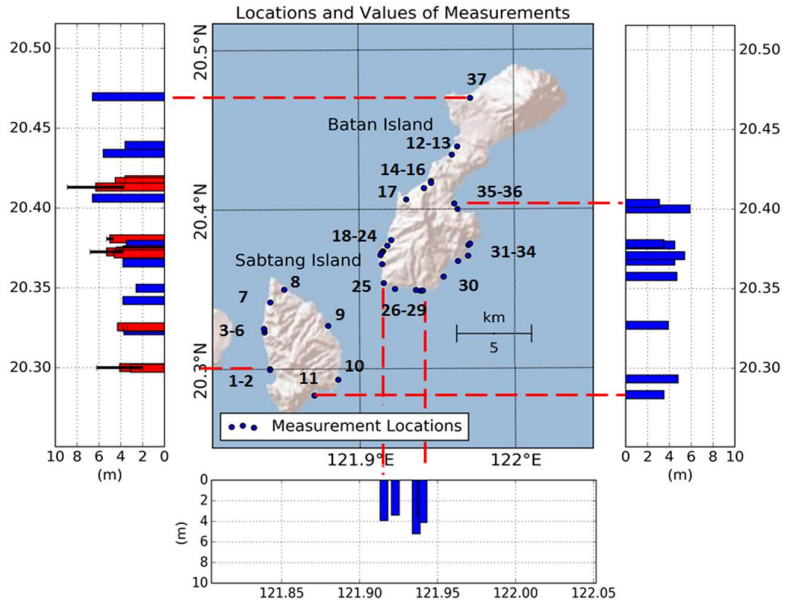

Figure 6. Locations and measured heights of wave runup (blue bars) and the water level in the inundated areas (red bars). Black bars indicate the witnessed range of fluctuating water level in the inundated area.

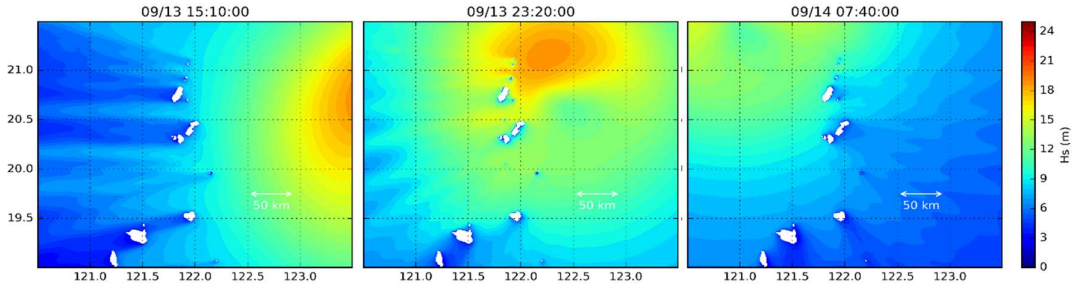

Figure 7. Significant wave height, H_s, distribution induced by typhoon Meranti at different times computed by WaveWatch III

numerical model is to explain how the two-dimensional geographic characteristics of the island influenced the local variation of the inundation levels.

4.1 Model Settings

To evaluate the refraction and diffraction effects around the island, a time-dependent, linear, mild-slope equations model for computing wave propagation was constructed. The governing equations of the model is from Berkhoff (1972)

$$\frac{\partial \eta}{\partial t} + \frac{1}{n}\nabla(n\boldsymbol{Q}) = 0 \tag{1}$$

$$\frac{\partial \mathbf{Q}}{\partial t} + C^2\frac{1}{n}\nabla(\eta) = 0 \tag{2}$$

where n is ratio of group velocity, C_g, and wave phase velocity, C. η is instantaneous water surface level an $\boldsymbol{Q}$ is the volume flux in the two horizontal dimensions. A sponge layer was used inside the surf zone and an open boundary condition was imposed at the shoreline to suppress the reflection of the incoming waves.

Finite difference method was used to numerically solve Eqs. 1 and 2. The computational domain was discretized according to the grid shown in Figure 8. The instantaneous water level η are defined at the cell nodes and the volume flux $\boldsymbol{Q}$ are defined at the midpoint of the cell edges. With this setting, the governing equations, Eqs. 1 and 2, can be discretized by second-order finite difference scheme equations. Adams predictor-corrector method was used in this model as the time-stepping scheme. The still water depth at each grid point was obtained from GEBCO's 30 arc-second interval grid global bathymetric data. The computational domain shown in Figure 8 is divided into 15m square grids and the timestep used in the calculations is 0.2s.

4.2 Model Results and Discussion

Unidirectional monochromatic waves were introduced to the computational domain from seven different directions: E, N 45° E, N 30° E, N, N 23° W, N 45° W, and W. These directions where chosen because the typhoon approached from the east direction and passed westward on the north side of the target island, Batan. The wave hindcast also revealed that the biggest waves approached the island from these directions. The incident wave height H_0 of the monochromatic wave introduced from each direction was initially set to be $H_0 = 1.0$ so that the wave height based on the computed η at each grid point corresponds to the combined refraction and diffraction coefficient. Figure 9 shows the spatial distribution of the combined refraction and diffraction effects around Batan Island under different incident wave angle conditions. Then, the coefficients at each survey location were extracted and plotted in Figure 10. The intermediate results shown in Figure 10 cannot be directly compared with the actual measured runup and inundations levels because the actual wave

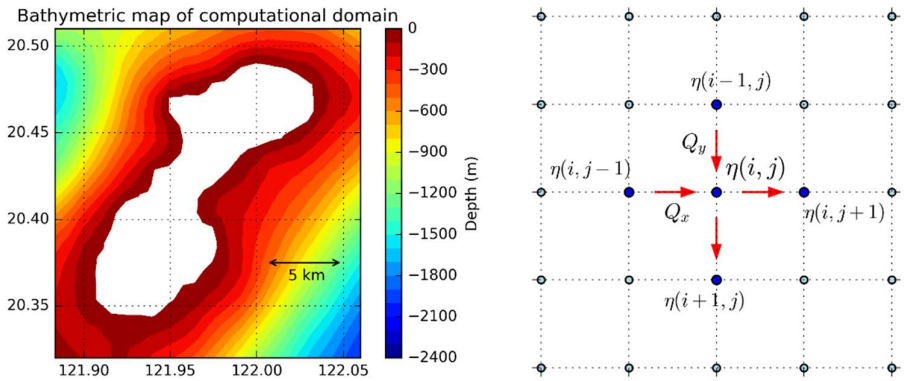

Figure 8. Computational domain and model grid setting

heights during the typhoon event varies at each direction of approach. So, the coefficients were re-computed and normalized according to the maximum wave height coming from each respective direction according to the wave hindcast done previously using WaveWatch III. The normalization was done by simple scalar multiplication since both the models are based on linear wave theory. After scaling the values in Figure 10, the trend of the refraction-diffraction coefficients is now amenable for comparison with the actual measured values. This result is presented in Figure 11, overlaid on top of the measured runup and inundation levels.

From Figure 11, It is seen that the alongshore variation of the measured runup and inundation levels generally follow the trend of the normalized combined refraction-diffraction coefficients, with the exception of survey points numbered 21-27 (underestimated), and 33-34, 36 (overestimated). This implies that the alongshore variation of the runup and inundation on all the other survey points are well described by the wave diffraction due to the natural topography of the island. The overestimation of the model on the survey points 33-34, and 36 is easily explained by the existence of breakwaters and other natural and artificial structures found at these locations which were not included in the numerical model. More interesting is the underestimation of the model at the survey points 21-27. This underestimation indicates that local wave amplification may have occurred due to the reefs around these survey points.

Among points that are underestimated, the points 21-23 are more peculiar because of their proximity to one another. All of these points are located in a small coastal village called Ivana. A closer look at these

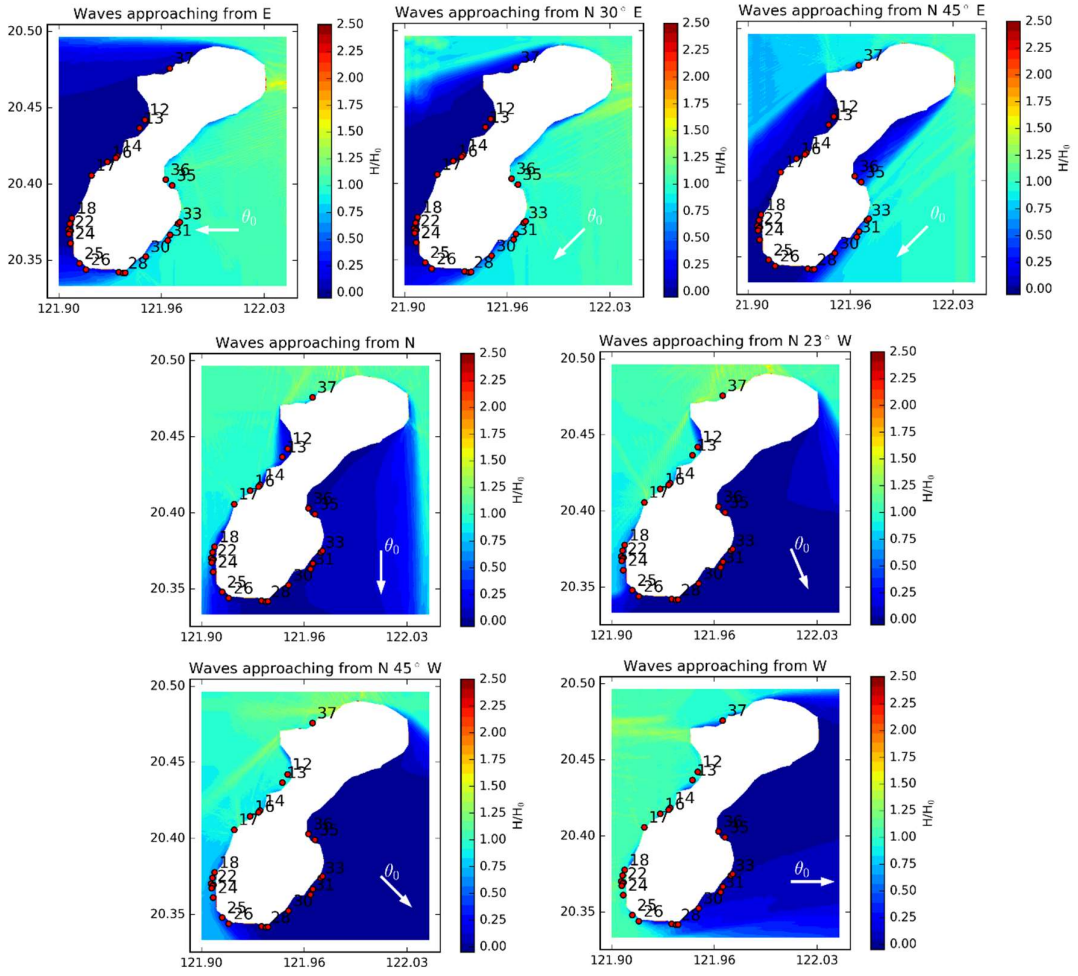

Figure 9. Computed combined refraction and diffraction effects around Batan Island upon introduction of monochromatic waves of unit height from different incident wave angles.

points, shown in Figure 12, reveals that the extreme inundation seems to have concentrated in a very small area. The highest inundation at Ivana measuring at 5.3 m with fluctuations up to 1.5 m was measured at point 22, near the tip of the convex-shaped reef with a narrow gap that serves as a navigation channel. It should further be noted that at the survey points 19 and 24 located at the north and south boundary of Ivana respectively, local residents witnessed no inundation. The reef width at points 19 and 24 are 76 m and 68 m respectively, much narrower than that at points 21-23 with 130 m, 141m, and 107 m wide fringing reefs. This supports the idea that the fringing reefs highly influenced the runup and inundation levels in this locality. Wave refraction at the reef edge or resonance of infragravity waves on the reef are offered as possible explanations for this observed wave amplification and concentration at Ivana. Further investigations are required for better understanding of the physical mechanisms of the locally concentrated inundation observed at Ivana.

5. Concluding Remarks

This study examined the locally varying characteristics of the wave runup and inundation along the coastlines of Batanes induced by Super Typhoon Meranti. More focus is given to the island of Batan which is almost entirely surrounded by shallow fringing reefs. Following the post-disaster survey of Tajima et al. (2017), which showed that the inundation and runup levels along the coast of Batanes have weak correlations with

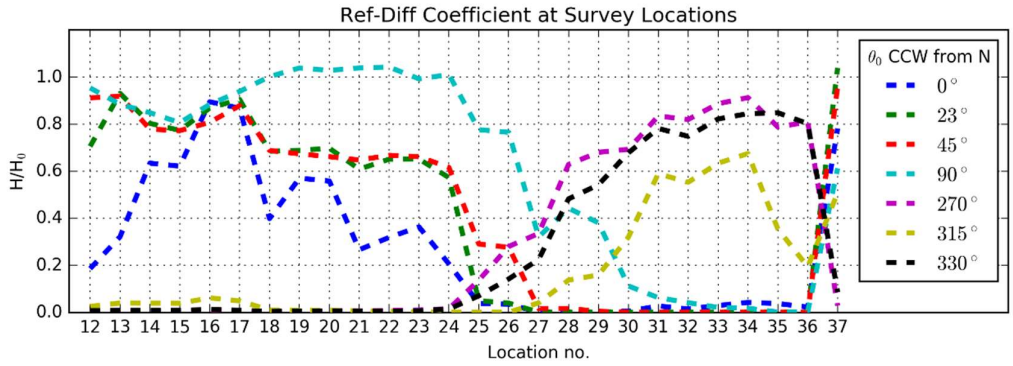

Figure 10. Trend line of the combined refraction-diffraction coefficients at the survey locations upon introduction of monochromatic waves of unit height from different incident wave angles.

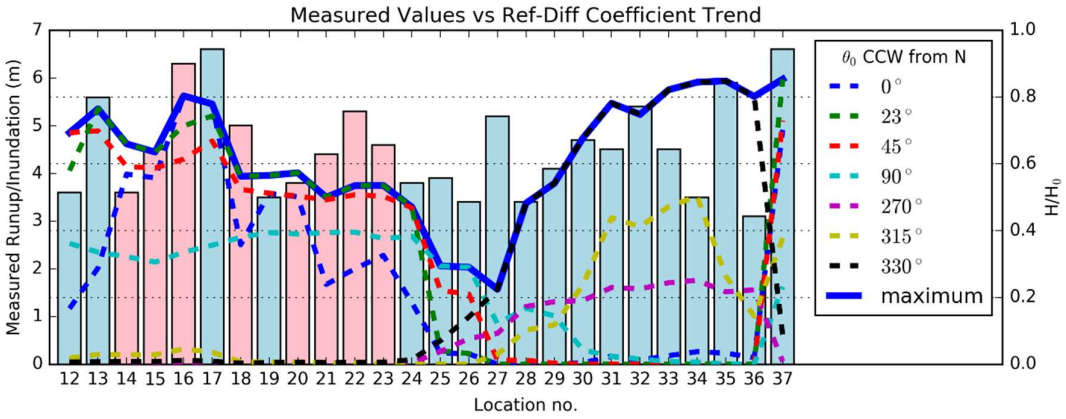

Figure 11. Trend line of the normalized combined refraction-diffraction coefficients overlaid on top of the measured runup (blue bars) and inundation (red bars) at the survey locations.

the reef width, this study proceeded by doing a detailed investigation of the refraction and diffraction effects of the natural topography of the island.

A wave hindcast was performed using WaveWatch III and a time-dependent, linear mild-slope equations model was constructed to simulate the combined two-dimensional wave refraction and diffraction around the island of Batan. It was found from the analysis that the trend of the alongshore variation of measured runup and inundation levels at most locations agrees well with the computed refraction-diffraction effects.

It was also found out that wave refraction and diffraction effects are not sufficient to account for the extreme inundation observed at some locations. This is especially apparent in Ivana, where wave amplification and wave concentration was observed in a very small area. The observed inundation heights were locally concentrated behind the widest segment of the convex-shaped fringing reef and near a narrow gap that is used as a navigation channel. It is suspected that resonance of infragravity waves on the reef flat is the reason for this phenomenon. Further analysis is suggested to be carried out focusing at Ivana or at the other localities fronted by fringing reefs where the model gave underestimated results.

Acknowledgements

The authors would like to gratefully acknowledge that a part of this work was supported by JSPS KAKENHI (B), Grant Number JP15H04046.

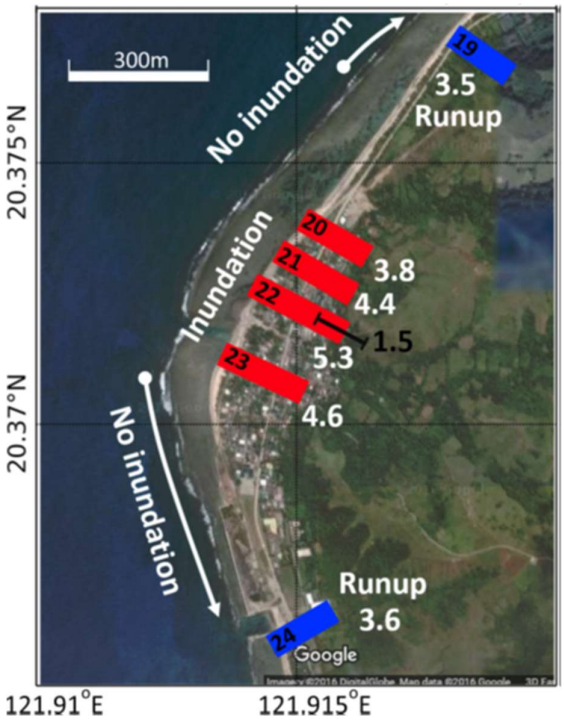

Figure 12. Measured heights of inundation (red bars) and wave runup (blue bars) and height fluctuation (black bar) along the coast of Ivana. The number in white letters are the measured heights from the MLWL and the numbers in black letters are the identification number of the location

References

Berkhoff, J. W., 1972. *Computation of Combined Refraction-Diffraction.* s.l., s.n., pp. 471-490.

Dunnavan, G. M. & Diercks, J. W., 1980. An Analysis of Super Typhoon Tip (October 1979). *Naval Oceanography Command Center/Joint Typhoon Warning Center, Guam 96630,* 29 July.pp. 1915-1923.

Hardy, T. A. & Young, I. R., 1996. Field study of wave attenuation on an offshore coral reef. *Journal of Geophysical Research,* 101(C6), pp. 14,311-14,326.

Joint Typhoon Warning Center, 2016. *Prognostic Reasoning for Typhoon 16W (Meranti) Warning NR 012-017,* s.l.: s.n.

Mitsuta, Y. & Fujii, T., 1987. Analysis and Synthesis of Typhoon Wind Pattern over Japan. *Bulletin of the Disaster Prevention Research Institute,* pp. 169-185.

Oey, L. Y. et al., 2006. Loop Current warming by Hurricane Wilma. *GEOPHYSICAL RESEARCH LETTERS,* Volume 33, p. L08613.

Pe´quignet, A. C., Becker, J. M., Merrifield, M. A. & Aucan, J., 2009. Forcing of resonant modes on a fringing reef during tropical. *GEOPHYSICAL RESEARCH LETTERS,* Volume 36, p. L03607.

Pe´quignet, A. C., Becker, J. M., Merrifield, M. A. & Boc, S. J., 2011. The dissipation of wind wave energy across a fringing reef at Ipan,. *Coral Reefs,* Volume 30, pp. 71-82.

Shimozono, T. et al., 2015. Combined infragravity wave and sea-swell runup over fringing reefs by super typhoon Haiyan. *Journal of Geophysical Research: Oceans,* Volume 120.

Tajima, Y. et al., 2017. Post-disaster survey of storm surge and waves along the coast of Batanes, the Philippines, caused by Super Typhoon Meranti/Ferdie. *Coastal Engineering Journal.*

Tajima, Y., Shimozono, T., Gunasekara, K. & Cruz, E., 2016. Study on Locally Varying Inundation Characteristics Induced by Super Typhoon Haiyan. Part 2: Deformation of Storm Waves on the Beach with Fringing Reef Along the East Coast of Eastern Samar. *Coastal Engineering Journal,* 58(1), p. 1640003.

Tajima, Y. et al., 2014. Initial Report of JSCE-PICE Joint Survey on the Storm Surge Disaster caused by Typhoon Haiyan. *Coastal Engineering Journal,* 56(1), p. 1450006.